

Reaction mechanism studies with 7–35 MeV/nucleon ${}^4\text{He}$ ions incident on heavy target nuclei

W. G. Meyer,* V. E. Viola, Jr., R. G. Clark,[†] and S. M. Read

Department of Chemistry and Cyclotron Laboratory, University of Maryland, College Park, Maryland 20742

R. B. Theus

U. S. Naval Research Laboratory, Washington, D. C.

(Received 6 June 1979)

Reaction mechanism studies have been performed on the ${}^4\text{He} + {}^{233}\text{U}$ system at energies of 7–35 MeV/nucleon and on the ${}^4\text{He} + {}^{209}\text{Bi}$ system at 12–35 MeV/nucleon. Measurements included (1) forward-angle elastic scattering, (2) angular distributions and total cross sections for fission, (3) fission-fragment angular correlations, and (4) fragment charge, mass, and energy distributions for ${}^{233}\text{U}(\alpha, f)$ at 140 MeV. Total inelastic cross sections and interaction radii were derived from the elastic scattering data. These values were found to be in good agreement with the total cross section for fission for the ${}^{233}\text{U} + {}^4\text{He}$ system, confirming the assumption that $\sigma_R \simeq \sigma_f$. Fission-fragment angular-correlation measurements were performed in order to deduce the distribution of linear momenta which characterize the residual heavy nuclei formed in these collisions. Complete linear momentum transfer probabilities (complete fusion) were also derived for both target-projectile systems as a function of energy. The data are compared with predictions of the proximity potential with one-body energy dissipation and with the intranuclear cascade code. The results of these comparisons are consistent with a picture in which complete fusion dominates the reaction mechanism below 10 MeV/nucleon, but pre-equilibrium processes assume increasing importance above this energy at the expense of fusion. In addition, evidence for a possible reduction in the interaction radius above 20 MeV/nucleon is reported.

NUCLEAR REACTIONS ${}^{209}\text{Bi}(\alpha, \alpha)$, ${}^{233}\text{U}(\alpha, \alpha)$, $E = 69.2, 140$ MeV, $\sigma_R(E)$;
 ${}^{209}\text{Bi}(\alpha, f)$, $E = 69.2, 140$ MeV, ${}^{233}\text{U}(\alpha, f)$, $E = 28\text{--}140$ MeV, $\sigma(\theta)$, $\sigma(E)$, fission-
 fragment angular correlations, Z and A distributions at 140 MeV; linear mo-
 mentum transfer to residual nucleus deduced; results compared with ion-ion
 potential models and intranuclear cascade code.

I. INTRODUCTION

The study of nuclear reactions induced by complex projectiles with energies between 10–100 MeV/nucleon has recently become the focus of considerable experimental and theoretical interest.^{1–3} This energy region is expected to be one of major transition, in which the principal reaction mechanisms evolve from relatively simple processes near the Coulomb barrier to the more complicated phenomena associated with high-energy collisions.

For relatively light complex projectiles incident on heavy target nuclei, reactions near the barrier are dominated by two major mechanisms: transfer processes associated with grazing collisions and complete fusion for smaller impact parameters. In either case the interaction potential is rarely sampled at radii for which there is an appreciable density overlap of the colliding nuclei. The transfer products are well described in terms of two-body final states in which the residual nucleus is produced in discrete states of excitation and acquires only a small component of the beam's linear momentum. Complete fusion, on the other

hand, involves total momentum transfer from the beam to the residual nucleus, and the light particle spectra associated with such events are characteristic of evaporation processes.

In contrast, at energies well above 100 MeV/nucleon the target-projectile interaction is characterized by a large multiplicity of nucleons and more complex fragments in the final state.⁴ Peripheral interactions at these energies have been explained in terms of a projectile fragmentation mechanism. For more central collisions, several models of rather different physics content are being employed to describe the single particle nucleon spectra. These include thermodynamic and hydrodynamic models, as well as intranuclear cascade, coalescence, and chemical equilibrium approaches to account for the composite particles.² It is not clear at this time which model is correct or whether the interactions represent a complicated mixture of all these processes. More definitive measurements are needed to answer these questions.

By studying the region between 10–100 MeV/nucleon one hopes to understand more fully the transition between these low- and high-energy

extremes. In addition, as the Fermi velocity (~ 20 MeV/nucleon) is exceeded, new nuclear phenomena may become observable.⁵ Although existing accelerators are limited in their ability to produce heavy-ion beams in this energy range, ^4He ions represent one complex projectile with which such studies can be readily pursued at the present time. Despite its few nucleon character, the alpha particle represents a tightly bound system which exhibits behavior analogous to heavy ions in many respects. Hence, reaction mechanism studies with ^4He ions should provide a valuable guide to the types of phenomena that will be observed with heavy ions with similar E/A values when the appropriate accelerators become available. In addition, such studies form an important comparative base from which anomalous behavior indicative of new reaction mechanisms may be deduced—once data from a wide variety of projectile-target systems are available.

The theoretical interpretation of nuclear reactions in the 10–100 MeV/ A transition region has relied principally on two models: (1) the pre-equilibrium exciton and related models,⁴⁻⁷ which apply to the low-energy portion of the region of interest, and (2) the intranuclear cascade model,⁸⁻¹² which is more appropriately used at the upper energy extreme. Despite the success of these models in describing some qualitative features of reactions above 10 MeV/nucleon, both models encounter difficulties in their treatment of reactions induced by complex projectiles because of their approximations relating to the ion-ion interaction potential. Recently, progress has been made in broadening these models for use with more complex projectiles.^{12,13}

In order to obtain a more quantitative understanding of the properties of projectilelike and residual heavy fragments formed in collisions between complex nuclei at lower energies, the use of phenomenological potentials plus one-body energy dissipation and diffusion mechanisms^{14,15} has proved quite valuable. However, at present these models lack the nucleon-nucleon collision features necessary to extend them to the description of reactions above 10 MeV/nucleon, especially when light-ion spectra are considered. In all probability the major features of each of these models will have to be incorporated into any successful theory for reactions induced by complex nuclei in the 10–100-MeV/nucleon range.

Experimental investigations of ^4He -ion induced reactions above 10 MeV/nucleon have shown a number of interesting features. Early studies of the distribution of residual nuclei in intermediate-energy ^4He -ion reactions demonstrated the importance of pre-equilibrium mechanisms for 10–

40-MeV/nucleon ^4He ions.^{16,17} A subsequent study with 35-MeV/nucleon ^4He ions incident on ^{238}U showed that a broad range of linear-momentum transfers characterized the residual heavy nuclei.¹⁸ Analysis of these data indicated that, at most, 50% of the reaction cross section results in complete fusion (defined here as complete-linear-momentum transfer). Another 40% of the reaction cross section was accounted for by reactions which involved the transfer of 50–90% of the projectile linear momentum to the target; these reactions were attributed to pre-equilibrium and deep knock-out processes. The remaining 10% of the reaction cross section could be described as peripheral reactions. Recent extensive studies of the light-ion spectra from 35-MeV/nucleon ^4He reactions with several targets by Wu *et al.*¹⁹ have substantiated these conclusions and greatly elucidated the mechanisms by which the projectile dissipates its energy. These results show clear evidence for many processes—including two-body final states, pre-equilibrium decay, projectile fragmentation, and evaporation products in ^4He -ion reactions. Recent heavy-ion studies have shown similar interesting features. Measurements of projectile like spectra for ^{16}O ions incident on heavy targets indicate a transition in reaction mechanisms near 20 MeV/nucleon,^{5,20} while linear-momentum-transfer determinations suggest the increasing importance of pre-equilibrium particle emission with increasing heavy-ion energy.^{21,22}

The purpose of the present work was to extend our earlier measurements by investigating the energy dependence of the linear-momentum transfer in reactions of ^4He ions with ^{233}U by means of the fission-fragment angular-correlation technique.¹⁸ The target ^{233}U was used in this work because of its high fissionability, which permits essentially complete definition of the reaction cross section in terms of fission, regardless of the amount of linear momentum transferred. In addition, the reaction models with which the data are compared are most appropriately applied to the heaviest systems possible. The results are examined both with the intranuclear cascade calculation, modified for ^4He projectiles, and with the predictions of models designed to account for heavy-ion reactions.

II. EXPERIMENTAL PROCEDURES

The experiments with 140-MeV alpha particles were performed at the Cyclotron Laboratory of the University of Maryland. Measurements with alpha particles between 28–70 MeV in energy were made at the U. S. Naval Research Laboratory Cyclotron Facility, Washington, D. C.

A 76-cm-diameter scattering chamber with remotely controlled movable arms and target ladder was used for each set of measurements. Isotopically pure (99.9%) ^{233}U and monoisotopic ^{209}Bi targets were prepared by vacuum evaporation onto $50\ \mu\text{g}/\text{cm}^2$ carbon. During all measurements the target was oriented at 45° with respect to the beam. A heavy-ion Si-surface-barrier detector was positioned at an angle of 135° to monitor the fission fragments from the reaction. The monitor was compared with the integrated beam current of the Faraday cup in order to ensure the consistency of all measurements. The integrated beam current (with an error of $\pm 5\%$ due to the absolute accuracy of the Faraday cup) was used for absolute normalization of the data.

Elastic scattering angular distributions of 140- and 69.2-MeV alpha particles from ^{233}U and ^{209}Bi were measured with a 4-mm Li-drifted-Si detector. The detector was tilted at an angle of 60° to the fragment normal and cooled to -10°C . The angular resolution was $\pm 0.5^\circ$ in all instances. Measurements were taken between 7° and 20° in angular steps of 1 to 2 degrees. A few measurements were also taken at representative angles on the opposite side of the beam axis in order to determine the absolute orientation of the beam as it passed through the scattering chamber.

Fission-fragment angular-distribution measurements were performed at alpha-particle energies of 27.5, 33.5, 43.8, 49.9, 58.9, 70.5, and 140

MeV for the $\alpha + ^{233}\text{U}$ system and at 69.2 and 140 MeV for the $\alpha + ^{209}\text{Bi}$ system. Measurements were performed in ten-degree steps from 10° to 170° . In addition, finer angular steps of 2 to 4 degrees were taken near 10° , 90° , and 170° to define the shape of the angular distribution in these regions. The fragment angular distributions were measured with a particle telescope consisting of two totally depleted silicon-surface-barrier transmission detectors (a $4\ \mu\text{m}$ thick ΔE and a $25\ \mu\text{m}$ thick E). The telescope had an angular acceptance of $\pm 0.5^\circ$ and measurements were made as close as 7° to the beam axis. The use of the $4\ \mu\text{m}$ detector aided the analysis of the fission-fragment angular-distribution data. Fission-fragment kinetic energy spectra were obtained that were completely separated from nonfission events, even at forward angles as close as 7° to the beam axis (as shown in Fig. 1). With partially depleted heavy-ion detectors which are normally used in fission-fragment detection, high-energy light particles deposit enough energy in the detector to cause an intense tailing into the fission-fragment energy spectrum. This effect leaves considerable uncertainty in the interpretation of the fission yield at forward angles, especially inside 30° .

The fission-fragment angular-correlation technique²³ was used to measure the angular correlation of binary fission fragments produced from alpha-particle interactions with ^{233}U and ^{209}Bi at bombarding energies of 49.0, 69.2, and 140

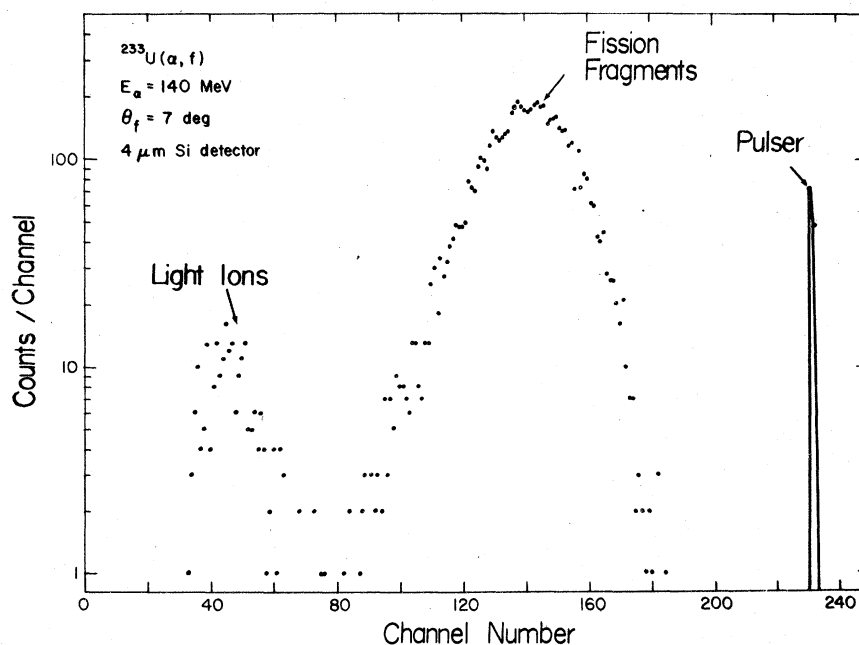


FIG. 1. Kinetic energy spectrum obtained with a $4\ \mu\text{m}$ totally depleted silicon-surface-barrier detector at a laboratory angle of 7° for the 140-MeV $\alpha + ^{233}\text{U}$ reaction.

MeV. The technique employed in these experiments involved the detection of coincident fission fragments with a particle telescope and a 50×6 -mm ion-implanted position-sensitive semiconductor detector (PSD). The telescope consisted of two silicon-surface-barrier detectors ($4 \mu\text{m} \Delta E$ and $25 \mu\text{m} E$) and was kept stationary at $+90^\circ$. The PSD was rotated between -90° and -78° in order to intercept the entire reaction plane. The particle telescope was collimated with a 0.48-cm-diameter aperture and the position detector was collimated with a 15-slit collimator. Slit dimensions for the rectangular slits were measured to be 0.10 cm wide by 0.47 cm high. The angular resolution of the particle telescope was $\pm 0.5^\circ$ and that of the PSD was $\pm 0.2^\circ$ in width and $\pm 1.1^\circ$ in height.

Measurements were made with both in-plane and out-of-plane orientations of the PSD. The in-plane measurements were made with the longitudinal axis of the PSD in the reaction plane (defined by the beam, target, and defining detector) and the out-of-plane measurements were made with the axis of the PSD perpendicular to the reaction plane. For each angular setting of the PSD, correlation measurements were made in both the in-plane and out-of-plane orientations for both the ^{233}U and ^{209}Bi targets. For the in-plane studies the telescope and PSD angles were kept constant for sequential measurement of the ^{233}U and ^{209}Bi targets. This procedure insured the systematic accuracy of all measurements and served as a check to the relative angular comparisons between the two targets.

A double time-of-flight (TOF), fission-fragment-fission-fragment correlation experiment was also performed on the $\alpha + ^{233}\text{U}$ system at 140 MeV. This measurement employed the particle telescope previously described, and a $75 \mu\text{m}$ (E_2) totally depleted silicon-surface-barrier detector. The ΔE and E detectors were located at distances of 6.8 and 34.4 cm, respectively, from the target, giving a fragment flight path of 26.7 cm. The location of the E_2 detector yielded a fragment flight path of 36.2 cm. Calibrations were made with a thin ^{252}Cf coincidence source. Measurements were performed at three fragment-fragment coincidence angles. At all three angles, the particle telescope was stationary at $+90^\circ$ while E_2 was rotated to angles of -90° , -78° , and -73° . The start time for the TOF measurement for both of the coincident fragments was derived from the E and E_2 detectors, respectively, operated in the inverted timing mode.

A block diagram of the experimental electronic configuration used in the angular-correlation measurements is shown in Fig. 2. A time-to-pulse-

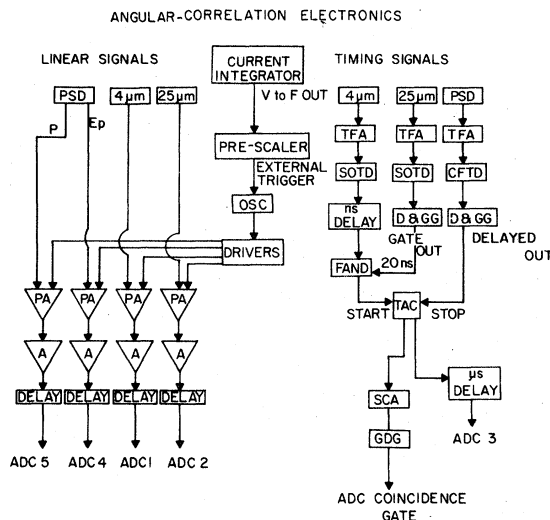


FIG. 2. Electronics schematic for angular-correlation measurements performed in these experiments. The linear signals were passed through standard preamplifier (PA), amplifier (A), and delay of circuits. Timing signals were processed via a timing-filter amplifier (TFA), timing discriminators (SOTD/CFTD), and time-to-amplitude converters (TAC). All analog-to-digital converter (ADC) outputs were then processed in an IBM 360/44 on-line computer.

height converter (TAC) was used to define a coincidence between the particle telescope and the PSD. The "start" and "stop" signals for the TAC were derived from a fast (20 nsec) ΔE - E coincidence and a fast time pickoff signal from the E preamplifier of the PSD, respectively. The five coincident signals—PSD energy and position, ΔE , E , and TAC—were stored sequentially on magnetic tape and analyzed off-line on an IBM 360-44 computer.

III. EXPERIMENTAL RESULTS

A. Interpretation of elastic scattering data

The elastic scattering measurements were performed to obtain a measure of the total inelastic cross section σ_R in order to test the assumption that σ_R is approximately equal to the cross section for fission σ_f for the $\alpha + ^{233}\text{U}$ system. In order to determine σ_R a semiclassical approach was used which employed Fresnel scattering theory. The choice of the Fresnel model was based on Frahn's criteria for classifying charged-particle scattering reactions.²⁴

Frahn has classified all charged-particle elastic scattering in terms of an η - h plot, where the Coulomb parameter η and the ratio of the center-of-mass kinetic energy to the Coulomb barrier h are given by

$$\eta = \frac{0.157}{E^{1/2}} Z_p Z_T \quad (1)$$

and

$$h = E \frac{A_p A_T}{Z_p Z_T} \frac{(A_p^{1/3} + A_T^{1/3})}{A_p + A_T} \quad (2)$$

Here $E = E_{\text{lab}}/A_p$ is the projectile laboratory energy in MeV/nucleon and the subscripts p and T refer to the projectile and target, respectively. Frahn also points out that two parameters, Λ and P , related to η and h by the following:

$$\begin{aligned} \Lambda &= 2\eta h(1 - h^{-1})^{1/2}, \\ P &= 2\eta[1 - (2h - 1)^{-2}], \end{aligned} \quad (3)$$

are generally needed to specify the type of scattering phenomenon with regard to its diffraction characteristics. Using the parameters Λ and P , Frahn distinguishes the following regions:

- (i) $\Lambda \leq 10$, nondiffractive scattering,
- (ii) $\Lambda \geq 10$, and $P \leq 0.1$, Fraunhofer scattering,
- (iii) $\Lambda \geq 10$, and $P \geq 1$, Fresnel scattering.

The ^{233}U and ^{209}Bi systems studied in this work fall well within the Fresnel region (iii).

In the Fresnel model the maximum angular momentum, l_{max} (where l_{max} is associated with the minimum impact parameter that leads to an elastic exit channel), for a given projectile-target interaction is given by

$$l_{\text{max}} = \eta \cot\left(\frac{\theta_{1/4}}{2}\right), \quad (4)$$

where $\theta_{1/4}$ is the "quarter-point" angle, i. e., the angle at which the experimental ratio of the elastic to the Rutherford cross section $\sigma_{e1}/\sigma_{\text{Ruth}}$ is equal to 0.25. The interaction radius R and reaction cross section σ_R are then given by

$$R = \frac{\eta}{k} \left[\text{cosec}\left(\frac{\theta_{1/4}}{2}\right) + 1 \right], \quad (5)$$

$$\sigma_R = \pi \lambda^2 (l_{\text{max}} + 1)^2, \quad (6)$$

where Eq. (4) is valid in the limit of large l_{max} values.

The quarter-point angle $\theta_{1/4}$ was determined by performing a least-squares fit to the experimental data at angles near the "grazing angle." The Fresnel parameters (η , l_{max} , σ_R , R , $\theta_{1/4}$) are

tabulated in Table I. The total reaction cross sections are found to be consistent with the σ_R values derived from an optical model fit to precision elastic scattering data for $^{208}\text{Pb} + 140\text{-MeV } ^4\text{He}$ -ion system.²⁵

B. Fission cross sections

The cross sections for fission as a function of projectile bombarding energy $\sigma_f(E)$ were determined from integration over the fission-fragment differential cross sections. The fragment differential cross sections were calculated from the integrated fission-fragment yield, the solid angle, the target thickness, and the integrated beam current. Integration of the differential cross sections was performed using a numerical integration method which employs a Simpson-rule technique with the Lagrangian four-point interpolation method. The fission cross sections for the ^{233}U and ^{209}Bi systems are listed in Table II. These values are in excellent agreement with the lower-energy values of Refs. 26-28.

The reaction cross sections derived from elastic scattering measurements for alpha particles incident on ^{233}U are compared with the fission cross sections in Table III and Fig. 3. This shows that the fission and inelastic cross sections agree well within the quoted limits of error; hence, we conclude that the assumption that $\sigma_R = \sigma_f$ is valid for the $\alpha + ^{233}\text{U}$ system. This is further substantiated by measurements of spallation residues for alpha-particle-induced reactions on ^{233}U and ^{235}U targets, which show that less than two percent of the inelastic cross section leads to the formation of targetlike residual nuclei over a broad energy range.^{29,30} For ^{209}Bi , which has a much higher fission barrier, the fission cross section is substantially less than the total inelastic cross section since only the highest linear-momentum-transfer components of σ_R lead to fission.

C. Fission-fragment angular correlation and complete-momentum-transfer cross sections

1. Angular-correlation function

The total angular-correlation functions for both the ^{209}Bi and ^{233}U systems were generated by first

TABLE I. Fresnel parameters for 69.2- and 140-MeV ^4He bombardment of ^{233}U and ^{209}Bi .

Reaction	E_{lab} (MeV)	$\theta_{1/4}$ (deg)	η	l_{max}	R (fm)	σ_R (mb)
$^4\text{He} + ^{233}\text{U}$	140.0	12.75	4.885	44	9.61	2450
	69.2	26.47	6.948	30	10.40	2290
$^4\text{He} + ^{209}\text{Bi}$	140.0	12.10	4.407	42	9.10	2250
	69.2	23.99	6.268	30	10.20	2290

TABLE II. Total fission cross sections for the $^{233}\text{U}(\alpha, f)$ and $^{209}\text{Bi}(\alpha, f)$ reactions.

Reaction	E_{lab} (MeV)	σ_f (mb)
$^4\text{He} + ^{233}\text{U}$	140.0	2490 ± 140
	70.5	2280 ± 150
	58.9	2210 ± 140
	49.9	2090 ± 130
	43.8	1700 ± 110
	38.5	1380 ± 90
	33.5	1110 ± 70
	27.5	628 ± 41
$^4\text{He} + ^{209}\text{Bi}$	140.0	1010 ± 80
	69.2	134 ± 11
	49.0	26 ± 2^a

^aReference 26.

converting all yields as a function of angle to differential cross sections $d^2\sigma/d\Omega_1 d\Omega_2$ for each in-plane and out-of-plane measurement. These cross sections were calculated from the yield, target thickness, integrated beam current, and the solid angles for each of the 15 slits of the position detector and the 4–25 μm ΔE - E telescope. The differential cross sections for all out-of-plane measurements were then fit with a Gaussian function of the form:

$$Y(\chi) = A \exp\left[-\frac{(\chi - \chi_0)^2}{2\sigma^2}\right], \quad (8)$$

where A is the height, χ_0 is the centroid, and σ^2 is the variance of the distribution. These normalized heights and variances were then used to determine the areas of each out-of-plane measurement as a function of each in-plane angle. The areas were computed numerically by integrating Eq. (8). The total correlation functions, projected onto the reaction plane, are presented in Fig. 4.

2. Complete-linear-momentum-transfer cross sections

Analysis of the data in Fig. 4 permits evaluation of the fraction of the total reaction cross section in which there is complete-linear-momentum transfer from the projectile to the struck nucleus, as well as definition of the distribution of linear momenta transferred in ^4He -ion reactions with

TABLE III. Comparison of fission cross sections with reaction cross sections derived from Fresnel scattering analysis.

E_{lab} (MeV)	σ_f (mb) [$\alpha + ^{233}\text{U}$]	σ_R (mb) [$\alpha + ^{233}\text{U}$]
140.0	2490 ± 140	2450 ± 110
69.2	2270 ± 150	2290 ± 100

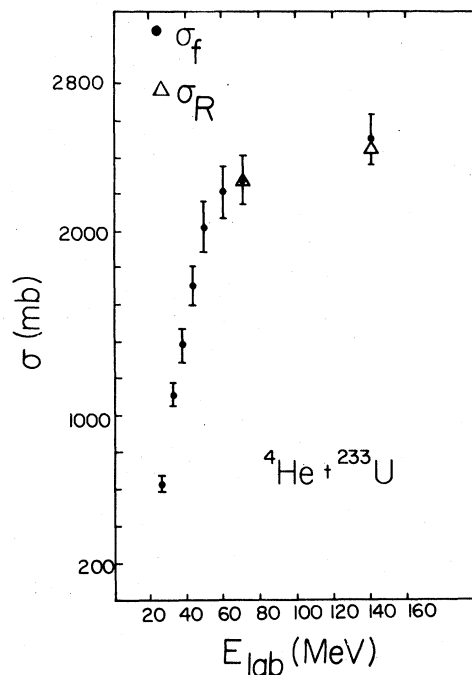


FIG. 3. Excitation function for the $^4\text{He} + ^{233}\text{U}$ system. Circles refer to fission cross section data; triangles represent total inelastic cross section data derived from elastic scattering.

heavy nuclei in this energy range. Reactions in which there is complete-linear-momentum transfer have generally been labeled complete fusion (cf) when applied to heavy-ion reactions.³¹ Since this definition is valid for the systems studied in this work, the symbol σ_{cf} is used to represent the complete-linear-momentum-transfer cross section. However, because it is not possible to distinguish uniquely between complete- and incomplete-linear-momentum-transfer processes in these reactions, we define σ_{cf} operationally to include all events which exhibit greater than 95% of complete-linear-momentum transfer. Hence, our quoted values for σ_{cf} represent an upper limit for the complete fusion cross section and may include some processes in which prompt, low-energy nucleon emission may have occurred.

In order to extract values for σ_{cf} from the $\alpha + ^{233}\text{U}$ data, the following procedure was followed. The fissioning nucleus was assumed to be ^{237}Pu with the maximum allowable excitation energy. The most probable mass split is known to be symmetric for these high excitation-energy fission cases (Ref. 32 and Sec. IIID), and the total kinetic energy release was calculated from semiempirical systematics.³³ The most probable center-of-mass (c.m.) transformation parameter χ_{mp} was then computed from two-body kinematics, using for the

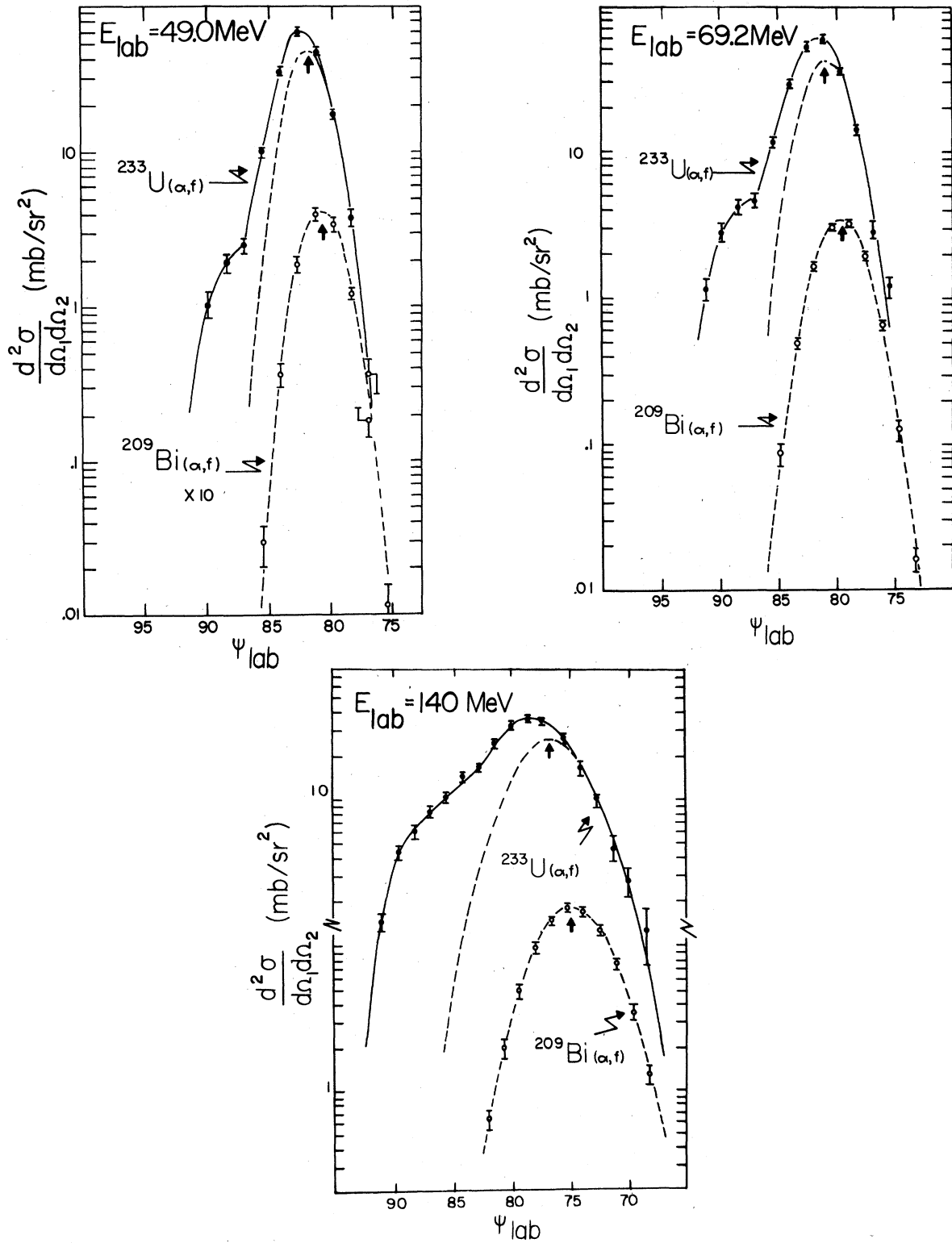


FIG. 4. Fission-fragment angular-correlation functions for the $^{233}\text{U}(\alpha, f)$ and $^{209}\text{Bi}(\alpha, f)$ reactions at 49.0, 69.2, and 140 MeV. The arrows indicate the position of the most probable correlation angle (ψ_{mp}) calculated from kinematics for complete-linear-momentum transfer. The dashed curves are fitted functions which indicate the fraction of complete-momentum-transfer events.

TABLE IV. Summary of fission-fragment angular-correlation parameters as described in text. The angular error was $\pm 0.24^\circ$ in the 140-MeV and 69.2-MeV bombardments; no absolute error normalization was made at 49.0 MeV.

Reaction	E_{lab} (MeV)	ψ_{mp} (deg) calculated	σ_{cf} (mb)	$\sigma_{\text{cf}}/\sigma_f$
$^4\text{He} + ^{233}\text{U}$	49.0	82.2	1468 ± 179	0.72 ± 0.09
	69.2	80.8	1376 ± 167	0.61 ± 0.07
	140.0	76.5	1342 ± 142	0.54 ± 0.05
$^4\text{He} + ^{209}\text{Bi}$	49.0	81.1	1509 ± 151	0.74 ± 0.07
	69.2	79.5	1344 ± 134	0.59 ± 0.06
	140.0	74.8	1399 ± 140	0.57 ± 0.06

Q value

$$Q = E_{\pi} - (E_{\text{lab}} A_T)/(A_P + A_T), \quad (9)$$

where E_{lab} is the laboratory kinetic energy of the projectile. The most probable laboratory correlation angle (ψ_2) for a fixed detector at a laboratory angle ψ_1 was calculated in the following manner. First the center-of-mass angle θ_1 was calculated from

$$\chi_{\text{mp}} = \frac{\sin(\theta - \psi)}{\sin\psi}. \quad (10)$$

Second, $\theta_2 = 180 - \theta_1$ was used with (10) and an iterative process to determine ψ_2 . The most probable correlation angle was calculated in this manner for all measurements made on both the ^{233}U and ^{209}Bi systems and the results are reported in Table IV. It should be noted that no corrections have been made for pre- or postfission neutron evaporation in calculations of χ_{mp} for the systems studied. Prefission neutron evaporation will slightly alter the values of χ_{mp} ; however, the effect is very small. Since postfission neutron evaporation is isotropic, it only affects the width of the angular-correlation function and not the most probable angle.

The ^{209}Bi total angular-correlation functions were found to be symmetric about the most probable correlation angle, as seen in Fig. 4 and previously reported by Viola *et al.*¹⁸ for the $\alpha + ^{209}\text{Bi}$ and $\alpha + ^{197}\text{Au}$ systems at 140 MeV. The ^{209}Bi functions were also found to be Gaussian in shape, indicating that incomplete-momentum-transfer events are not a significant contribution to the fission cross section.

Based on the ^{209}Bi results, the correlation functions for the $\alpha + ^{233}\text{U}$ system were used to obtain values of σ_{cf} by means of the following procedure. The differential cross sections for lowest angles ψ (corresponding to maximum momentum transfer) of each ^{233}U correlation function in Fig. 4 were fitted with the Gaussian function [Eq. (8)], where $x_0 = \psi_{\text{calc}}$ was entered as an input parameter and

was only allowed to vary within the limits of the angular error for each measurement. The results of this analysis are shown in the form of the dashed curves in Fig. 4 and represent the complete-linear-momentum-transfer component of the reaction cross section quoted here.

The fraction of complete-momentum-transfer events was taken to be the ratio of the numerical integral of Eq. (8) (using the results for A , x_0 , and σ^2 obtained from the fitting procedure) to the numerical integral of the total correlation function. This ratio times the total fission cross section is defined as the cross section for complete-momentum transfer σ_{cf} . The results of these calculations are presented in Table IV.

Values of σ_{cf} for the $\alpha + ^{209}\text{Bi}$ system were determined from the sum of $(\alpha, xn)^{213-x}$. At excitation functions based on Refs. 17 and 34 and the fission cross sections in Table II. These are also listed in Table IV. As in the case of the $^{233}\text{U} + \alpha$ system, the quoted σ_{cf} values represent an upper limit due to: (1) the (α, xn) cross sections may include a small amount of low-energy pre-equilibrium neutron emission, and (2) despite the concordance of the fission angular-correlation function for ^{209}Bi with that expected for complete fusion, a finite component of incomplete-momentum-transfer cannot be ruled out. However, it is estimated that these errors are less than 15% of the quoted σ_{cf} values. The values of σ_{cf} obtained for ^{209}Bi and ^{233}U in this manner are found to be in good agreement with one another (Table IV).

3. Summary

From Table IV it is apparent that even at the relatively low energy of 12 MeV/nucleon, a substantial fraction of the reaction cross section does not result in complete-linear-momentum transfer. With increasing energy the fraction of incomplete-momentum-transfer events increases, so that at 35 MeV/nucleon, nearly half the reaction cross section is consumed by such events, in good agree-

ment with previous work at this energy.¹⁸ Figure 4 also demonstrates that the distribution of linear-momentum transfer in these intermediate-energy ${}^4\text{He}$ -ion reactions is a continuous function at all bombarding energies. Of particular importance, there is a major contribution of large, but incomplete-, linear-momentum-transfer events to the total reaction cross section. Presumably, these are associated with pre-equilibrium processes accompanied by the emission of relatively low-energy particles.¹⁹ In Sec. IV these results are discussed further in terms of specific nuclear reaction models.

D. Most probable Z and A of fission products

The double-time-of-flight (TOF), ΔE - E measurements were performed to determine the most probable charge $\langle Z \rangle$ and mass $\langle A \rangle$ of the fission products as a function of linear momentum transferred from the projectile to the fissioning nucleus.

The mass (A) of the fission fragments was determined by

$$A = \frac{ax + b}{0.5v^2 - a'x - b'}, \quad (12)$$

where the constants a , a' , b , and b' are given by the expression

$$E(x, A) = (a + a' - A)x + b'A, \quad (13)$$

and x is the pulse height and v is the velocity of the fragment. The coefficients a , a' , b , and b' were determined as described by Schmitt³⁵ from a ${}^{252}\text{Cf}$ calibration of the E detector. The velocity $v = D/T$ was computed from the fragment flight distance D and flight time T , where $T = T_0 - \text{TAC}$. The constant T_0 was determined from the calculated flight times for the most probable light and heavy fragments of ${}^{252}\text{Cf}$.

The fission-fragment charge was computed after Bowman *et al.*³⁶

$$Z \propto PI/A^{(b-1)/2}, \quad (14)$$

where

$$PI = [(\Delta E + E)^P - (E)]^{1/2}, \quad (15)$$

and

$$P = b - \frac{c}{t} \frac{\Delta E}{E}. \quad (16)$$

Here b and c are constants and t is the ΔE detector thickness. A numerical search was performed to determine the values of the constants b and c such that Eq. (14) would properly reproduce the most probable Z of both the light and heavy peaks of ${}^{252}\text{Cf}$.

In Fig. 5 we show the mass versus charge con-

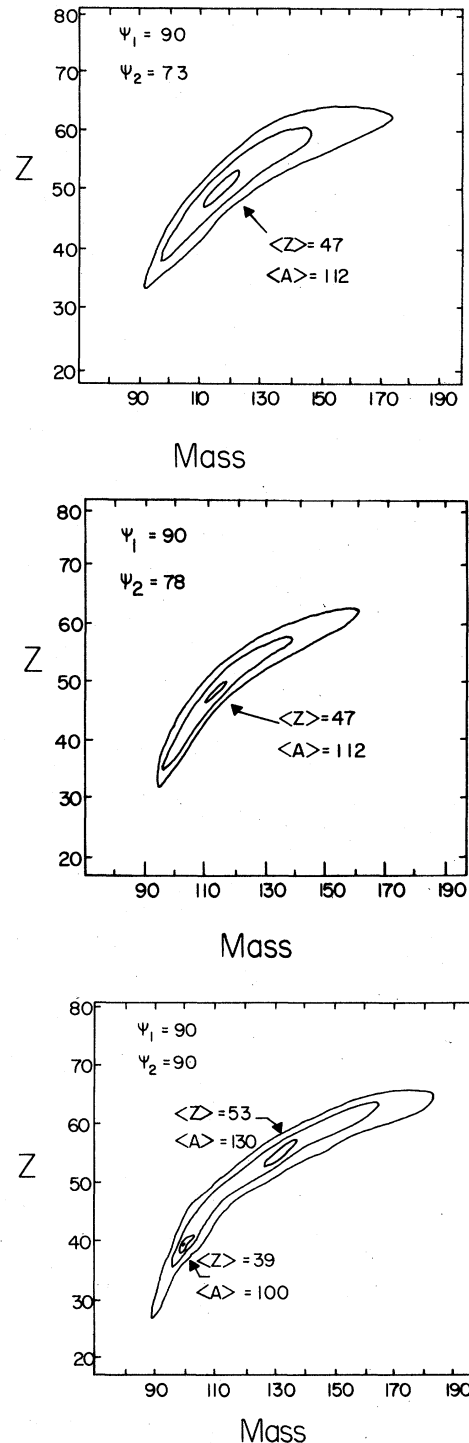


FIG. 5. Charge versus mass contours for binary fission events observed at various correlation angles for the bombardment of ${}^{233}\text{U}$ with 140-MeV ${}^4\text{He}$ ions. The data were obtained with a semiconductor ΔE - E time-of-flight telescope as described in Sec. II for the following angles between the two fragments: (a) 163° , (b) 167° , and (c) 180° .

tours for fission fragments at three different correlation angles: (a) 163° , corresponding to complete-linear-momentum transfer, (b) 167° , corresponding to large, but incomplete transfer, and (c) 180° , corresponding to zero momentum transfer.

In cases 5(a) and 5(b) the mass and charge distributions show the symmetric division expected of high excitation-energy fission. In addition for the most probable fragment charge and mass, we obtain $\langle Z \rangle = 47$ and $\langle A \rangle = 112$, characteristic of fission from a ^{237}Pu compound nucleus. Energy balance calculations predict that approximately 6-7 neutrons should be emitted from each excited fission fragment in these cases, which completes the mass balance. Thus, these data corroborate the conclusions of the angular-correlation data that fission coincidences observed at strongly forward-folded angles originate in equilibrated systems, where complete (or nearly complete) fusion has occurred in the target-projectile interaction.

In Fig. 5(c) the mass-charge contour for colinear events exhibits a much different character. The fission process is clearly asymmetric in this case, indicative of low excitation-energy fission. Here the total most probable charge $\langle Z_H \rangle + \langle Z_L \rangle = 92$ and the total most probable mass $\langle A_H \rangle + \langle A_L \rangle = 230$, which implies fission from an average residual nucleus such as ^{234}U (assuming two neutrons are emitted from each fragment). Hence, these fission fragments are interpreted in terms of direct processes in which there is little mass transfer and the struck nucleus is left in a very low state of excitation prior to equilibration and fission.

IV. DISCUSSION

A. Qualitative aspects of the cross sections

It was shown in Sec. IIIA that to a very good approximation the assumption that $\sigma_f = \sigma_R$ is valid for $^4\text{He} + ^{233}\text{U}$ interactions up to a ^4He energy of 35 MeV/nucleon. In order to examine the dependence of σ_R and σ_α on bombarding energy, it is useful to construct a plot of cross section versus $1/E_{\text{c.m.}}$ as shown in Fig. 6. Here we have plotted fission cross sections for the $^4\text{He} + ^{233}\text{U}$ system obtained at low energies^{26,27} along with the values of σ_f and σ_α determined in this work. The arrows indicate two important threshold energies:

(1) 10 MeV/nucleon—where pre-equilibrium effects are believed to become important,^{7,16,17,37} and

(2) 20 MeV/nucleon—approximately the Fermi energy for nucleons in complex nuclei.

From inspection of Fig. 6, several features of

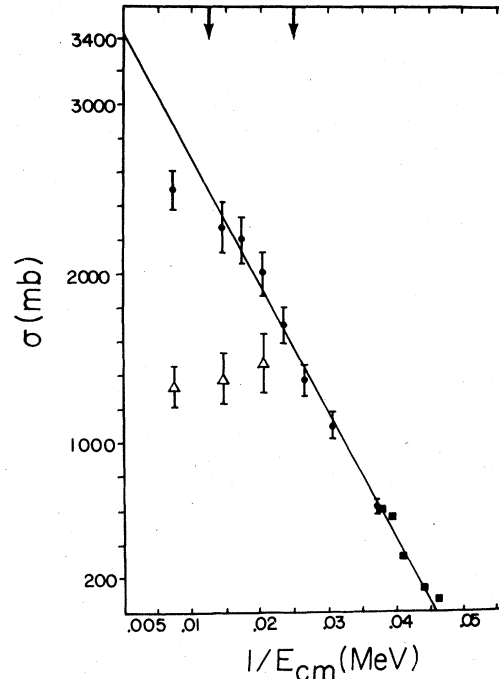


FIG. 6. Plot of cross section (in mb) as a function of the reciprocal of the projectile center-of-mass energy. Symbols have the following meaning: \blacksquare —fission cross section data from Ref. 27; \bullet —fission cross section data from this work, and Δ —complete fusion cross sections from this work. It is assumed that the fission cross section is identical to the total inelastic cross section in these comparisons. The solid line represents a least-squares fit to the fission cross sections below 70 MeV based on Eq. (14).

the data require comment. First, at low projectile energies ($1/E_{\text{c.m.}} \gtrsim 0.025$) earlier spallation cross section and angular-correlation measurements have demonstrated that the fission, complete fusion, and total inelastic cross sections are essentially identical^{26,29,38} and depend linearly on $1/E_{\text{c.m.}}$. The data in Fig. 6 have been fitted in an analogous fashion to Scobel *et al.*³⁹ with the function

$$\sigma_R = \pi R^2 (1 - V_B/E_{\text{c.m.}}), \quad (14)$$

where R is the interaction radius and V_B is the interaction barrier. The solid line in Fig. 6 represents a least-squares fit of this function to the data for σ_R up to 70 MeV. The interaction radius determined in this manner is 10.4 fm, which is nearly identical to the value of R_{int} derived from the Fresnel analysis of the 69.2 MeV data (Table I). A value of V_B of 22 MeV is also obtained, in good agreement with a recent analysis by Birkelund and Huizenga.⁴⁰

Second, for bombarding energies in excess of 10 MeV/nucleon it is noted that the complete fusion

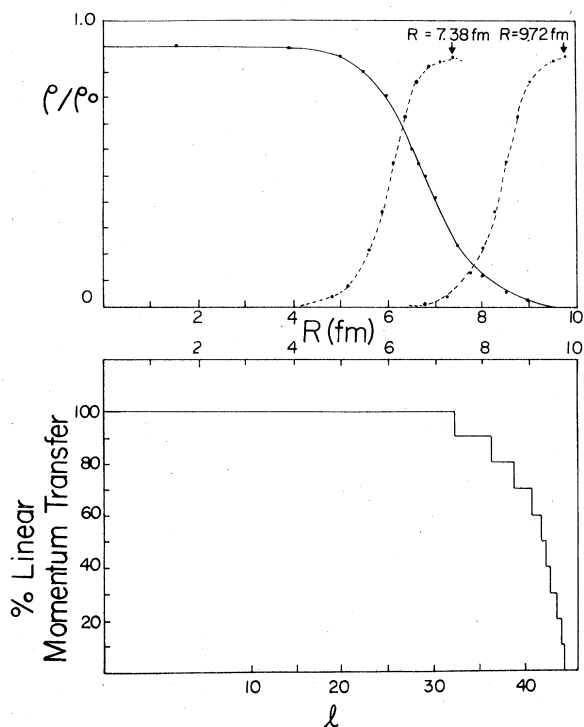


FIG. 7. (a) Lower figure shows the percentage of complete-linear-momentum-transfer events as a function of orbital angular momentum, assuming the highest l waves are responsible for incomplete fusion processes. The relation between l and R is determined by Eqs. (4) and (5) and is not valid for low l values ($\lesssim 10$). (b) Upper figure shows plot of ratio of nuclear density to the central density for ^{233}U (solid line) and ^4He (dashed line) for separation distances corresponding to the interaction barrier (9.72 fm) and complete-linear-momentum transfer (7.38 fm).

cross section and the total inelastic cross section diverge markedly. The total inelastic cross section continues to depend linearly on $1/E_{\text{c.m.}}$, whereas σ_{el} flattens out and actually decreases with increasing energy. To aid in understanding this transition, in Fig. 7(a) we have constructed a plot which relates the linear-momentum-transfer distribution characteristic of σ_R in the 140-MeV $\alpha + ^{233}\text{U}$ system to the interaction radius and orbital angular momentum involved in the reaction. The cross section corresponding to a given linear-momentum transfer was derived as described in Ref. 18 and the relationship between σ , R_{int} , and l was determined using Eqs. (4), (5), and (6). The assumption upon which Fig. 7(a) is based is that the largest linear-momentum-transfer events are associated with the smallest impact parameters and that the linear-momentum trans-

fer decreases smoothly for increasingly peripheral reactions. In Fig. 7(b) we show the nuclear density overlap⁴¹ between ^4He and ^{233}U nuclei for separation distances of 9.72 fm (corresponding to the total inelastic cross section) and 7.38 fm (corresponding to the complete fusion cross section). This schematic analysis is consistent with a picture in which reactions occurring in the tail of the nuclear density distribution lead to direct, incomplete-momentum-transfer processes, whereas once a density overlap greater than about 70% occurs, complete-linear-momentum transfer follows.

This deviation between σ_{el} and σ_R is well known in heavy-ion reactions and has been explained in terms of various models which employ the concept of a critical angular momentum^{15,42,43} or a critical distance of approach for the colliding ions.⁴⁴ Because of the relatively low values of angular momentum associated with alpha-particle reactions (e.g., for 140-MeV ^4He ions, $l_{\text{max}} \sim 44\hbar$, and the fusion cross section corresponding to $l_{\text{crit}} \sim 33\hbar$), it is not clear to what extent these models apply to ^4He -ion reactions. This aspect of the data is discussed in greater detail in the following section.

Finally, the deviation in the total inelastic cross section as a function of $1/E_{\text{c.m.}}$ at 140 MeV constitutes an additional point of interest. In terms of Eq. (14) this cross section corresponds to an interaction radius of 9.72 fm, about 8% smaller than that consistent with the value of 10.4 fm indicated by the solid curve in Fig. 6. This deviation suggests that at sufficiently high energy, the interaction radius may contract; i.e., greater overlap between the target and projectile density distributions may be required to produce an inelastic collision. It is of interest to note that this point is near the Fermi energy—20 MeV/nucleon—also shown in Fig. 6. The implication of this argument is that once the projectile velocity exceeds the velocity of the nucleons inside the nucleus, interactions between the projectile nucleons and those of the target are less efficient in transferring energy. Hence, the available interaction volume is reduced. Clearly, additional data are needed to investigate this effect. The same qualitative dependence of σ_R on $1/E_{\text{c.m.}}$ is seen in proton-nucleus interactions, as shown in Fig. 8 for proton bombardment of a lead target.^{45,46} In this case σ_R reaches a maximum at an energy just above the Fermi energy and then falls to an asymptotic value for energies greater than 200 MeV. This behavior is analogous to the proton-proton interaction, where the decrease in σ_R above 100 MeV is attributed to transparency effects.

B. Comparison with interaction models

In an effort to understand these data in more quantitative terms, we have compared these results with existing models for collisions between complex nuclei, specifically the proximity potential which includes one-body energy dissipation¹⁴ and the intranuclear cascade model.^{11,13} Although neither model is designed to describe the energy region spanned by the present study, the comparison is made in the spirit of providing guidelines for future development of intermediate-energy, complex nucleus reaction theory. In Fig. 9 we have compared the complete fusion cross sections of Table IV with the predictions of the proximity potential.⁴⁷ The dashed curve represents the prediction of the proximity potential with no energy dissipation included. It is observed that this form of the model predicts a slope for the high-energy portion of the fusion cross section that is much too steep; predicted cross sections in the 40–100 MeV region are too high while that at 140 MeV is low by a factor of 2.

A more realistic approach is to consider the effects of one-body energy dissipation, which will serve to increase the fusion cross section by damping radial motion of the projectile into excitation of the system. The dotted line in Fig. 9 shows such a prediction for the model of Birkelund

*et al.*¹⁴ which fits a large body of heavy-ion fusion data. In this comparison it is observed that the calculated fusion cross sections greatly exceed the experimental values. Since in many respects the proximity potential resembles the measured optical model potential,⁴⁸ it is also of interest to compare our results with the fusion cross section predicted by the optical model, assuming all l waves for which an attractive total potential exists lead to fusion. In this comparison we have scaled the optical model potential for the 140-MeV ${}^4\text{He} + {}^{208}\text{Pb}$ system²⁵ to ${}^{233}\text{U}$. This exercise yields a complete fusion cross section comparable to that of the proximity potential with one-body energy dissipation.

We interpret the difference between our experimental results and the proximity and optical potential model predictions to be consistent with the onset of two-body energy dissipation mechanisms at bombarding energies above 10 MeV/nucleon. As these processes assume increasing importance with respect to nucleon-potential scattering (one-body energy dissipation), the emission of light (pre-equilibrium) particles becomes increasingly probable. These processes thus lead to a light-ion component in the distribution of product nuclei which exhibits a broadly damped energy spectrum¹⁹

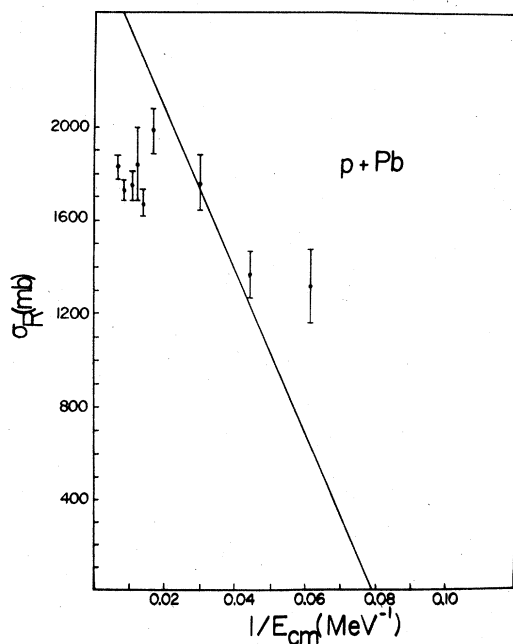


FIG. 8. Plot of total inelastic cross section versus $1/E_{c.m.}$ for the proton plus lead system; based on data of Refs. 45 and 46. The solid line represents a calculation based on Eq. (14), using $r_0 = 1.34$ fm.

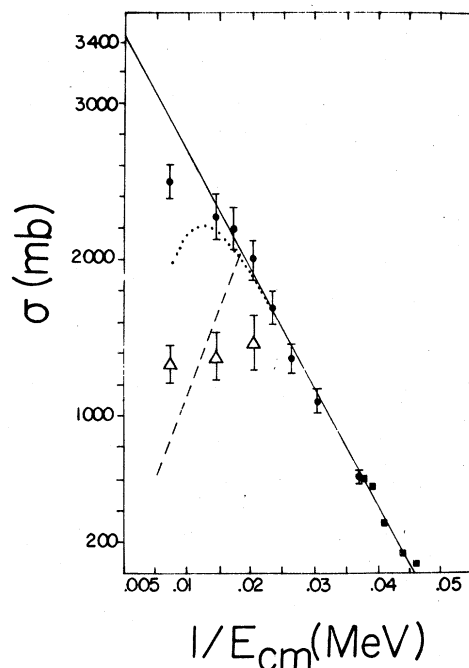


FIG. 9. Data shown in Fig. 6 are compared with calculations based on the proximity potential. The dashed line represents the complete fusion cross section prediction of the proximity potential with no energy dissipation. The dotted line shows the same predictions for a calculation which includes one-body energy dissipation.

and yields residual nuclei with large but incomplete-linear-momentum transfer.

With increasing bombarding energy, these effects should become increasingly dominant. In the previously discussed models the specific features of two-body energy dissipation are omitted. Hence, collisions in which direct nucleon (or light-ion) emission occurs—with a concurrent loss in linear momentum for the targetlike residual—are integrated into the complete fusion process, thereby yielding too high a calculated fusion cross section. It is interesting to note that if one considers the experimental cross section for all events in which the linear-momentum transfer is greater than 50%, then rather good agreement with these interaction potential calculations is obtained. Hence, we conclude that there is no serious disagreement with the present calculations, but that in order to describe reactions with complex nuclei above 10 MeV/nucleon more completely, one must include two-body energy dissipation mechanisms and consider the effect of such processes on the definition of complete fusion.

In view of the above interpretation, it is of interest to compare the present experimental results with the predictions of the intranuclear cascade code, which explicitly includes two-body energy dissipation. The code of Chen *et al.*¹¹ has recently been modified to permit calculations for reactions induced by deuterons and alpha particles, as well as for the existence of *d* and α clusters in the target nucleus.¹³ In Fig. 10 the experimental fission-fragment angular correlation for 140-MeV alpha particles incident on ²³³U is plotted along with predictions of the intranuclear cascade code. The calculations assumed one alpha-particle cluster in the ²³³U target (not a very sensitive parameter) and did not allow for refraction and reflection at the nuclear surface.¹¹ Two assumptions were made concerning alpha-particle collisions in the cascade: one which permitted the alpha particle to break up and the other which allowed no breakup. From the linear-momentum-transfer distribution and corresponding excitation energies predicted for the residual heavy nuclei, the fission-fragment angular correlation was then calculated. This calculation included dispersion effects due to neutron emission from the fragments.

Qualitatively, the calculations reproduce the basic features observed in the data, i. e., distinct complete (or nearly so) fusion and peripheral components, plus a substantial fraction of events that are characterized by a large, but incomplete-linear-momentum transfer. Clearly, the no-breakup assumption for alpha-particle cascades provides a better fit to the data. However, since

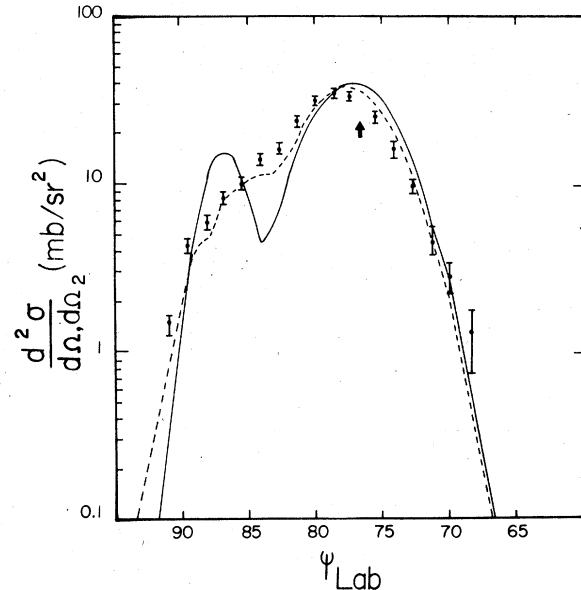


FIG. 10. Comparison of the experimental fission-fragment angular correlations at 140 MeV with predictions based on the intranuclear cascade model. The solid line refers to cascades which allow alpha-particle breakup; the dashed line refers to a no-breakup assumption.

the treatment of the ion-ion potential is very approximate in the intranuclear cascade model, one cannot expect to reproduce the exact details of the data with such a calculation, especially at the low energies for which the model is applied here. Nonetheless, the calculations do reinforce the previous conclusion that the effects of two-body energy dissipation must be incorporated into models which hope to describe collisions induced by complex nuclei above 10 MeV/nucleon.

V. CONCLUSIONS

In summary, we have investigated the bombarding-energy dependence of the linear-momentum transfer in ⁴He collisions with heavy nuclei. Above an energy of 10 MeV/nucleon it is observed that a significant fraction of the total inelastic cross section involves reactions in which there is incomplete-linear-momentum transfer from projectile to target nucleus. This behavior becomes more pronounced with increasing bombarding energy up to 35 MeV/nucleon. The distribution of momentum transfer is a continuous function that is weighted toward high (>50%), but incomplete, momentum transfer, indicating a strong projectile-target interaction. The complete fusion (>95% complete-momentum-transfer) cross section decreases slightly above 10–12 MeV/nucleon. Also, it is noted that at the highest bombarding

energies, the total inelastic cross section σ_R falls well below the predicted geometric limit. This appears to indicate a shrinkage of the interaction radius at bombarding energies above the Fermi energy, an effect which needs further investigation.

Attempts to account for the fusion (complete-momentum-transfer) cross section in terms of a proximity potential model which includes one-body energy dissipation are unsatisfactory. The same is true for other existing models currently used to account for fusion cross sections in heavy-ion reactions, as well as with a scaled optical potential based on elastic scattering measurements. However, both the proximity and optical models do agree well for events in which there is greater than 50% linear-momentum transfer, i. e., collisions in which there is a strong target-projectile interaction. Also, attempts to account for the linear-momentum-transfer distribution with a cluster intranuclear cascade model are qualitatively reasonable.

This analysis emphasizes the increasing importance of two-body energy dissipation in interaction above 10 MeV/nucleon, where the energy equilibration process leads to the ejection of nu-

cleons (and clusters) with a wide range of outgoing energies. Thus, as the onset of pre-equilibrium particle emission begins to dominate the inelastic cross section, one expects to observe a wide range of momentum transfers to the struck nucleus and increasingly complex spectra for the emitted light particles.

ACKNOWLEDGMENTS

This work was supported by the U. S. Department of Energy, the National Science Foundation, and the U. S. Naval Research Laboratory. The authors wish to express their gratitude for many helpful discussions of these data with D. A. Goldberg, J. R. Huizenga, and D. Sperber. We are indebted to B. G. Glagola for performing the intranuclear cascade model calculations and to the University of Maryland Computer Center for support of these computations. We also wish to thank the operating crews of the cyclotrons at the University of Maryland and the U. S. Naval Research Laboratory for their assistance with these experiments. One of us (VEV) wishes to acknowledge the University of Maryland for providing a University Research Professorship during the writing of this paper.

*Present address: Bell Laboratories, Reading, Pa.

†Present address: U.S. Department of Energy, Washington, D.C.

¹Proceedings of the Topical Conference on Heavy-Ion Collisions, Fall Creek Falls, Tennessee, 1977, U. S. Department of Commerce Report No. CONF-770602, 1977.

²Proceedings of the Fourth Summer Study in High-Energy Heavy-Ion Physics, Berkeley, 1978, LBL Report No. 7766, 1978.

³J. P. Bondorf, *J. Phys. (Paris)* **37**, C5 (1976).

⁴G. D. Westfall, J. Gosset, P. J. Johansen, A. M. Poskanzer, W. G. Meyer, H. H. Gutbrod, A. Sandoval, and R. Stock, *Phys. Rev. Lett.* **37**, 1202 (1976); **37**, 667 (1976); *Phys. Rev. C* **16**, 629 (1977).

⁵D. K. Scott, LBL Report No. 7111, 1977.

⁶J. J. Griffin, *Phys. Rev. Lett.* **17**, 478 (1966); *Phys. Lett.* **24B**, 15 (1967).

⁷M. Blann, *Annu. Rev. Nucl. Sci.* **25**, 123 (1975).

⁸A. Mignerey, M. Blann, and W. Scobel, *Nucl. Phys.* **A273**, 125 (1976).

⁹R. Serber, *Phys. Rev.* **72**, 1114 (1947).

¹⁰M. L. Goldberger, *Phys. Rev.* **74**, 1269 (1948).

¹¹V. S. Barashenkov, H. W. Bertini, K. Chen, G. Friedlander, G. D. Harp, A. S. Iljinov, J. M. Miller, and V. D. Toneev, *Nucl. Phys.* **A187**, 531 (1972); K. Chen, Z. Fraenkel, G. Friedlander, J. R. Grover, J. M. Miller, and Y. Shimamoto, *Phys. Rev.* **166**, 949 (1968).

¹²J. M. Akkermans, *Phys. Lett.* **82B**, 20 (1979); see also

R. K. Smith and M. Danos, Ref. 1, p. 363.

¹³R. A. Moyle, G. J. Mathews, B. G. Glagola, and V. E. Viola, University of Maryland Report No. ORO-5172-4, 1979, to be published.

¹⁴J. R. Birkelund, J. R. Huizenga, J. N. De, and D. Sperber, *Phys. Rev. Lett.* **40**, 1123 (1978).

¹⁵D. H. E. Gross and H. Kalinowski, *Phys. Lett.* **48B**, 302 (1974); J. N. De, D. H. E. Gross, and H. Kalinowski, *Z. Phys.* **A277**, 385 (1976).

¹⁶F. M. Lanzafame and H. Blann, *Nucl. Phys.* **A142**, 545 (1970).

¹⁷R. Bimbot and Y. Lebevec, *J. Phys. (Paris)* **32**, 18, 243 (1971).

¹⁸V. E. Viola, C. T. Roche, W. G. Meyer, and R. G. Clark, *Phys. Rev. C* **10**, 2416 (1974).

¹⁹J. R. Wu, C. C. Chang, and H. D. Holmgren, *Phys. Rev. Lett.* **40**, 1013 (1978); J. R. Wu, C. C. Chang, and H. D. Holmgren, *Phys. Rev. C* **19**, 659, 698 (1979).

²⁰C. K. Gelbke, C. Olmer, M. Buenerd, D. C. Hendrie, J. Mahoney, M. C. Mermaz, and D. K. Scott, *Phys. Rep.* **42**, 311 (1978).

²¹P. Dyer, T. C. Awes, C. K. Gelbke, B. B. Back, A. Mignerey, K. L. Wolf, H. Breuer, V. E. Viola, and W. G. Meyer, *Phys. Rev. Lett.* **42**, 545 (1979).

²²V. E. Viola, R. G. Clark, W. G. Meyer, A. M. Zebelman, and R. G. Sextro, *Nucl. Phys.* **A261**, 174 (1976).

²³W. J. Nicholson and I. Halpern, *Phys. Rev.* **116**, 175 (1959); M. M. Minor, V. E. Viola, A. E. Salwin, R. B. Theus, and R. O. Bondelid, *Nucl. Instrum. Methods* **99**,

- 63 (1972).
- ²⁴W. E. Frahn, Phys. Rev. Lett. 26, 568 (1971); W. E. Frahn, Ann. Phys. (N.Y.) 72, 524 (1972).
- ²⁵D. A. Goldberg, S. M. Smith, H. G. Pugh, P. G. Roos, and N. S. Wall, Phys. Rev. C 7, 1938 (1973); D. A. Goldberg, private communication.
- ²⁶A. Kodai-Joopari, Lawrence Berkeley Laboratory Report No. UCRL-16489, thesis (unpublished) (1966).
- ²⁷J. R. Huizenga, private communication.
- ²⁸S. S. Kapoor, H. Baba, and S. G. Thompson, Phys. Rev. 149, 965 (1966).
- ²⁹R. Vandenbosch, T. D. Thomas, S. E. Vandenbosch, R. A. Glass, and G. T. Seaborg, Phys. Rev. 111, 1358 (1958).
- ³⁰P. A. Schuster and V. E. Viola, Jr. (unpublished).
- ³¹S. Cohen, F. Plasil, and W. J. Swiatecki, Ann. Phys. (N.Y.) 82, 557 (1974).
- ³²E. W. Frick, University of Maryland Report No. MNC-4028-0016, thesis (unpublished) (1974).
- ³³V. E. Viola, Nucl. Data A1, 391 (1966).
- ³⁴J. D. Stickler and K. J. Hofstetter, Phys. Rev. C 9, 1064 (1974).
- ³⁵H. W. Schmitt, W. E. Kiker, and C. W. Williams, Phys. Rev. 137, B837 (1965).
- ³⁶J. D. Bowman, A. M. Poskanzer, R. G. Korteling, and G. W. Butler, Phys. Rev. C 9, 836 (1974).
- ³⁷D. G. Sarantites, L. Westerberg, M. L. Halbert, D. A. Dayras, D. C. Hensley, and J. H. Barker, Phys. Rev. C 18, 774, 796 (1978).
- ³⁸T. Sikkeland, E. L. Haines, and V. E. Viola, Phys. Rev. 125, 1350 (1962).
- ³⁹W. Scobel, H. H. Gutbrod, M. Blann, and A. Mignerey, Phys. Rev. C 14, 1808 (1976).
- ⁴⁰J. R. Birkelund and J. R. Huizenga, Phys. Rev. C 17, 126 (1978).
- ⁴¹C. W. de Jager, H. de Vries, and C. de Vries, At. Data Nucl. Data Tables 14, 479 (1974).
- ⁴²J. Wilczyński, Nucl. Phys. A216, 386 (1973).
- ⁴³R. Bass, Nucl. Phys. A231, 45 (1974).
- ⁴⁴C. Ngô, B. Tamain, J. Galin, M. Beiner, and R. J. Lombard, Nucl. Phys. A240, 343 (1975).
- ⁴⁵R. E. Pollock and G. Schank, Phys. Rev. 140, B575 (1964) and references therein.
- ⁴⁶D. J. Ernst, Phys. Rev. C 19, 896 (1979).
- ⁴⁷J. Blocki, J. Randrup, W. J. Swiatecki, and C. F. Tsang, Ann. Phys. (N.Y.) 105, 427 (1977).
- ⁴⁸S. Tabor, D. A. Goldberg, and J. R. Huizenga, Phys. Rev. Lett. 41, 1285 (1978).